Engineering local strain for single-atom nuclear acoustic resonance in silicon ⊘

Laura A. O'Neill; Benjamin Joecker; Andrew D. Baczewski; ... et. al

Check for updates

CrossMark

View
Online

Export
Citation

Articles You May Be Interested In

Engineering local strain for single-atom nuclear acoustic resonance in silicon

View Online   Export Citation   CrossMark

Laura A. O'Neill,[1] (iD) Benjamin Joecker,[1] (iD) Andrew D. Baczewski,[2] and Andrea Morello[1,a)] (iD)

AFFILIATIONS

[1]School of Electrical Engineering and Telecommunications, UNSW Sydney, Sydney, New South Wales 2052, Australia
[2]Center for Computing Research, Sandia National Laboratories, Albuquerque, New Mexico 87123, USA

Note: This paper is part of the APL Special Collection on Emerging Qubit Systems - Novel Materials, Encodings and Architectures.
[a)]Author to whom correspondence should be addressed: a.morello@unsw.edu.au

ABSTRACT

Mechanical strain plays a key role in the physics and operation of nanoscale semiconductor systems, including quantum dots and single-dopant devices. Here, we describe the design of a nanoelectronic device, where a single nuclear spin is coherently controlled via nuclear acoustic resonance (NAR) through the local application of dynamical strain. The strain drives spin transitions by modulating the nuclear quadrupole interaction. We adopt an AlN piezoelectric actuator compatible with standard silicon metal–oxide–semiconductor processing and optimize the device layout to maximize the NAR drive. We predict NAR Rabi frequencies of order 200 Hz for a single ^{123}Sb nucleus in a wide region of the device. Spin transitions driven directly by electric fields are suppressed in the center of the device, allowing the observation of pure NAR. Using electric field gradient-elastic tensors calculated by the density-functional theory, we extend our predictions to other high-spin group-V donors in silicon and to the isoelectronic ^{73}Ge atom.

Published under an exclusive license by AIP Publishing. https://doi.org/10.1063/5.0069305

Mechanical strain is a key design parameter for modern solid-state devices, both classical and quantum. In classical microelectronics, strain is used to increase carrier mobility and has been crucial in advancing device miniaturization.[1] Strained heterostructures can confine highly mobile two-dimensional electron gases,[2] which are used both in classical high-frequency devices and in quantum applications such as quantum dots,[3–5] quantum Hall devices,[6] and topological insulators.[7] It is well established that local strain strongly affects the properties of gate-defined quantum dots[8–10] and dopants in silicon.[11–14]

The above examples pertain to static strain. Dynamic strain and its quantized limit (phonons) constitute instead the "next frontier" of hybrid quantum systems.[15] Circuit quantum acoustodynamics[16] aims at hybridizing acoustic excitations with other quantum systems on a chip. Pioneering experiments coupled superconducting qubits to localized acoustic modes of mechanical resonators[17] or traveling modes of surface acoustic waves.[18] Proposals exist for hybridizing phonons with the valley-orbit states of donors in silicon.[19] Recent efforts include the coherent drive of spins in solids, such as diamond[20–24] and silicon carbide,[25] and the strong coupling between magnons and phonons.[26] Phononic quantum networks[27] can be designed to link acoustically driven quantum systems.

In this paper, we assess the possibility of controlling the quantum state of a single nuclear spin using dynamic mechanical strain, i.e., the nuclear acoustic resonance (NAR) of a single atom. NAR was observed long ago in bulk antiferromagnets[28] and semiconductors.[29,30] It is a very weak effect, and its development has been essentially abandoned after 1980s. However, the recent demonstration of nuclear electric resonance (NER) in a single ^{123}Sb nuclear spin in silicon[31] shows that it is possible to coherently drive a nuclear spin by resonant modulation of the electric field gradient (EFG) $\mathscr{V}_{ij}$ ($i, j = x, y, z$) at the nucleus. Here, we study the case where the EFG is caused by a time-dependent local strain ε_{ij} produced by a piezoelectric actuator. The relation between EFG and strain is described by the gradient-elastic tensor S, which was also obtained from the NER experiment in Ref. 31. We expand our analysis by using S values obtained from *ab initio* density functional theory (DFT) models, covering the ^{75}As, ^{123}Sb, and ^{209}Bi donor nuclei and the isoelectronic ^{73}Ge element.

Consider a nuclear spin I with gyromagnetic ratio γ_n, placed in a static magnetic field $B_0 \parallel z$. For the purpose of this discussion, we assume that the nucleus is isolated, i.e., it is not hyperfine- or dipole-coupled to an electron. A coupled electron is necessary during the readout phase[32] but can be removed at all other times. The isolated nucleus is described in the basis of the states $|m_I\rangle$, $m_I = -I \cdots I - 1, I$, representing the projections of the spin along the z-axis, i.e., the eigenvectors of the Zeeman Hamiltonian (in frequency units)

$$\hat{H}_{Z} = -\gamma_n B_0 \hat{I}_z. \tag{1}$$

For nuclei with $I > 1/2$, a static EFG couples to the electric quadrupole moment q_n via the Hamiltonian

$$\hat{H}_{Q} = \frac{eq_n}{2I(2I-1)h} \sum_{i,j} \mathscr{V}_{ij} \hat{I}_i \hat{I}_j, \tag{2}$$

where e is the elementary charge and h is Planck's constant. The quadrupole interaction splits the nuclear resonance frequencies $f_{m_I-1 \leftrightarrow m_I}$ between pairs of eigenstates as

$$f_{m_I-1 \leftrightarrow m_I} = \gamma_n B_0 + \left(m_I - \frac{1}{2} \right) \frac{eq_n}{2I(2I-1)h} \left(\mathscr{V}_{xx} + \mathscr{V}_{yy} - 2\mathscr{V}_{zz} \right) \tag{3}$$

and allows addressing individual transitions. Spin transitions can be driven not only by standard nuclear magnetic resonance (NMR) but also by resonant modulation of the EFG via the off diagonal Hamiltonian

$$\delta\hat{H}_{Q} = \frac{eq_n}{2I(2I-1)h} \sum_{i,j} \delta\mathscr{V}_{ij} \hat{I}_i \hat{I}_j, \tag{4}$$

where $\delta\mathscr{V}_{ij}$ denotes the amplitude of the time-varying EFG.

For $\Delta m_I = \pm 1$ transitions, the nuclear quadrupolar Rabi frequency $f_{m_I-1 \leftrightarrow m_I}^{\text{Rabi}} = |\langle m_I - 1 | \delta\hat{H}_Q | m_I \rangle|$ simplifies to

$$f_{m_I-1 \leftrightarrow m_I}^{\text{Rabi}} = \frac{e|q_n|}{2I(2I-1)h} \alpha_{m_I-1 \leftrightarrow m_I} |\delta\mathscr{V}_{xz} + i\delta\mathscr{V}_{yz}|, \tag{5}$$

where $\alpha_{m_I-1 \leftrightarrow m_I} = |\langle m_I - 1 | \hat{I}_j \hat{I}_z + \hat{I}_z \hat{I}_j | m_I \rangle|$ for $j = x, y$.

In the case of NAR, a time-dependent strain $\delta\varepsilon_{ij}$ periodically deforms the local charge environment of the nucleus and creates an EFG modulation described by the gradient-electric tensor S. This effect depends on the host crystal and its orientation with respect to the coordinate system, in which S is defined. For the T_d symmetry of a substitutional lattice site in silicon, S is completely defined by two unique elements S_{11} and S_{44}. In Voigt's notation and with the Cartesian axes aligned with the $\langle 100 \rangle$-crystal axis, e.g., $z \parallel [100]$, $x \parallel [010]$, and $y \parallel [001]$

$$\begin{pmatrix} \delta\mathscr{V}_{xx} \\ \delta\mathscr{V}_{yy} \\ \delta\mathscr{V}_{zz} \\ \delta\mathscr{V}_{yz} \\ \delta\mathscr{V}_{xz} \\ \delta\mathscr{V}_{xy} \end{pmatrix} = \begin{pmatrix} S_{11} & \frac{-S_{11}}{2} & \frac{-S_{11}}{2} & 0 & 0 & 0 \\ \frac{-S_{11}}{2} & S_{11} & \frac{-S_{11}}{2} & 0 & 0 & 0 \\ \frac{-S_{11}}{2} & \frac{-S_{11}}{2} & S_{11} & 0 & 0 & 0 \\ 0 & 0 & 0 & S_{44} & 0 & 0 \\ 0 & 0 & 0 & 0 & S_{44} & 0 \\ 0 & 0 & 0 & 0 & 0 & S_{44} \end{pmatrix} \cdot \begin{pmatrix} \delta\varepsilon_{xx} \\ \delta\varepsilon_{yy} \\ \delta\varepsilon_{zz} \\ 2\delta\varepsilon_{yz} \\ 2\delta\varepsilon_{xz} \\ 2\delta\varepsilon_{xy} \end{pmatrix}, \tag{6}$$

where the factor 2 in the shear components arises, because the S-tensor is defined with respect to engineering strains. Crucially, for a magnetic field $B_0 \parallel z$ aligned with a $\langle 100 \rangle$ crystal orientation, Eqs. (5) and (6) yield the NAR driving frequency

$$f_{m_I-1 \leftrightarrow m_I}^{\text{Rabi,NAR}} = \alpha_{m_I-1 \leftrightarrow m_I} \frac{e|q_n|}{2I(2I-1)h} 2S_{44} \sqrt{\delta\varepsilon_{xz}^2 + \delta\varepsilon_{yz}^2}, \tag{7}$$

which exclusively depends on shear strain components that couple to the EFG via S_{44}. Rotating the magnetic field away from the principal crystal axis, e.g., $z \parallel [110]$, would increase the contribution of uniaxial strain components, proportional to S_{11}. Since $S_{44} > S_{11}$ in all cases (see Table I), the strongest acoustic drive is obtained when $B_0 \parallel \langle 100 \rangle$.

A dynamic EFG can also be created by a time-dependent electric field δE_i, which distorts the bond orbitals coordinating the donor. This process, leading to NER,[31] is described by the R-tensor

$$\begin{pmatrix} \delta\mathscr{V}_{xx} \\ \delta\mathscr{V}_{yy} \\ \delta\mathscr{V}_{zz} \\ \delta\mathscr{V}_{yz} \\ \delta\mathscr{V}_{xz} \\ \delta\mathscr{V}_{xy} \end{pmatrix} = \begin{pmatrix} 0 & 0 & 0 \\ 0 & 0 & 0 \\ 0 & 0 & 0 \\ R_{14} & 0 & 0 \\ 0 & R_{14} & 0 \\ 0 & 0 & R_{14} \end{pmatrix} \cdot \begin{pmatrix} \delta E_x \\ \delta E_y \\ \delta E_z \end{pmatrix}. \tag{8}$$

Notably, the resulting NER driving frequency,

$$f_{m_I-1 \leftrightarrow m_I}^{\text{Rabi,NER}} = \alpha_{m_I-1 \leftrightarrow m_I} \frac{e|q_n|}{2I(2I-1)h} R_{14} \sqrt{\delta E_x^2 + \delta E_y^2}, \tag{9}$$

only depends on electric field components perpendicular to $B_0 \parallel z$. In a device where NAR is driven by a piezoelectric actuator, the time-varying strain is necessarily accompanied by a time-varying electric field, but the above observations will allow us to engineer a layout that maximizes NAR while largely suppressing NER.

We, thus, propose the device structure as shown in Fig. 1. It is similar to the standard layout adopted in metal-oxide-semiconductor (MOS) compatible single-donor devices in silicon,[34,35] including a single-electron transistor (SET) for electron spin readout via spin-to-charge conversion,[36] an on-chip microwave antenna[37] to drive electron[38] and nuclear[32] spin resonance transitions, and electrostatic gates to locally control the potential in the device. The same gates, connected to control lines with $\sim$100 MHz bandwidth, can be used to deliver oscillating electric fields.[31] A group-V donor or an isoelectronic center with nuclear spin $I > 1/2$ is introduced by ion implantation. To address the isoelectronic center like ^{73}Ge, the structure should further include a lithographically defined quantum dot[39] to host an additional

TABLE I. Parameters and results for different donors with nuclear spin $I > 1/2$. The nuclear gyromagnetic ratios and quadrupole moments are extracted from Ref. 53, where a range of values for q_n are reported. The uniaxial S_{11} and shear S_{44} components of the gradient elastic tensor [see Eq. (6)] were calculated using DFT. The resulting quadrupole splitting f_Q [Eq. (10)] is given for a donor located in the center of the implantation region at depth $y = -5$ nm. The corresponding NAR Rabi frequencies [Eq. (7)] are reported for the $m_I = I - 1 \leftrightarrow I$ transition.

	^{75}As	^{123}Sb	^{209}Bi	^{73}Ge
I	3/2	7/2	9/2	9/2
γ_n (MHz/T)	7.31	5.55	6.96	−1.49
q_n (10^{-28} m^2)	0.314	−0.69	−0.77	−0.17
S_{11} (10^{22}V/m^2)	2.3	2.0	4.5	0.2
S_{44} (10^{22}V/m^2)	4.1	5.9	12.0	3.3
$|f_Q|$ (kHz)	50	14	20	0.2
$f_{m_I-1 \leftrightarrow m_I}^{\text{Rabi,NAR}}$ (Hz)	92	190	380	23
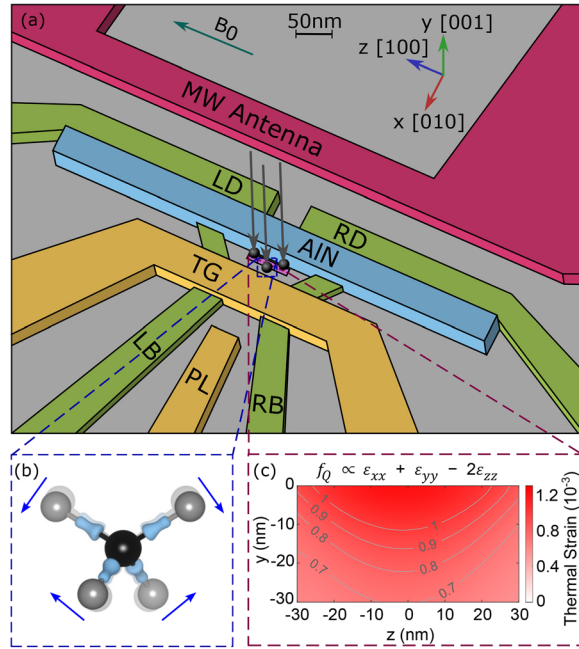
FIG. 1. (a) Device geometry for nuclear acoustic resonance, based upon standard donor qubit devices but modified to include a 55 nm thick piezoelectric actuator (AlN, blue). A single-electron transistor is formed by an electron gas induced by the top gate (TG, yellow) and controlled by the plunger gate (PL, yellow), left and right barriers (LB, RB, green). Left and right donor gates (LD, RD, green) control the donor electrochemical potential. The piezoactuator creates a time-dependent strain when applying a radio frequency voltage $V_{RF}\cos{(2\pi f_{m_I-1\leftrightarrow m_I}t)}$ to LB, LD, and $-V_{RF}\cos{(2\pi f_{m_I-1\leftrightarrow m_I}t)}$ to RB and RD. A microwave antenna (magenta) is used to induce magnetic resonance transitions as necessary for nuclear spin readout via an electron spin ancilla. A static magnetic field B_0 is assumed applied along the $z \equiv [100]$ axis. The design assumes the center of the 60(W)x30(H)x10(D) nm^3 implantation window is located 30 nm from the top gate TG. (b) Sketch (generated using VESTA[33]) of strain-induced atomic bond distortion for a substitutional donor (black) in silicon (gray). (c) Distribution of static strain in the device, caused by differential thermal expansion. We plot the components $\varepsilon_{xx} + \varepsilon_{yy} - 2\varepsilon_{zz}$ responsible for the nuclear quadrupole splitting f_Q [Eq. (10)].

electron, hyperfine-coupled to the nucleus, as recently demonstrated with ^{29}Si.

We introduce two changes to the standard layout. First, we include a strip of piezoelectric materials, placed on top of the implantation region between the gates and the SET, to create a time-dependent local strain $\delta\varepsilon_{ij}$ upon application of an oscillating voltage V_{RF} to the gates. Second, we align the piezoelectric and the gates with the [100] crystal direction, along which a static external magnetic field $B_0 \sim 1$ T is applied (z-axis). This requires rotating the device layout by 45° compared to standard donor devices, where B_0 and gates are aligned along [110],[40] which is the natural cleaving face for silicon wafers.

We model the device geometry in the modular COMSOL multiphysics software. A $2 \times 2 \times 2 \, \mu m^3$ silicon substrate is capped by an 8 nm thick SiO$_2$ layer. The aluminum gates, covered by 2 nm of Al$_2$O$_3$ through oxidation, and the piezoelectric actuator are placed on top. We use the "AC/DC Module" to compute the electrostatics, the "Structural Mechanics Module" for thermal deformation, and combined multiphysics simulations for the piezoelectric coupling. The static strain ε_{ij}, resulting from the difference in thermal expansion coefficients among different materials, is modeled as described in Ref. 31. An 8 nm thick SiO$_2$ dielectric is grown at 850 °C and is assumed strain-relaxed at that temperature. The Al gates and AlN piezoelectric are subsequently deposited and subjected to a forming gas anneal that strain-relaxes them at 400 °C. The whole stack is then cooled to the device operating temperature of 0.2 K. Figure 1(c) shows the components of the static strain that cause the splitting f_Q between nuclear resonance frequencies in Eq. (3)

$$f_Q = \frac{eq_n}{2I(2I-1)h}\frac{3}{2}S_{11}(\varepsilon_{xx} + \varepsilon_{yy} - 2\varepsilon_{zz}). \qquad (10)$$

In the center of the implantation region, near the Si/SiO$_2$ interface, we predict $|f_Q| = 14$ kHz for the ^{123}Sb nucleus (see Table I for other nuclei), ensuring that the resonance lines are well resolved. In the electrostatic simulations, the idle gate voltages are set to $V_{LB} = 0$ V, $V_{RB} = 0$ V, $V_{PL} = 0$ V, $V_{TG} = 1.8$ V, $V_{LD} = 0$ V, $V_{RD} = 0$ V, and $V_{MW} = 0$ V. Additionally, we ground the Si/SiO$_2$ interface under the SET to model the effect of the conducting electron channel.[34,36] The COMSOL material library conveniently provides all other parameters.

We choose aluminum nitride (AlN) as the piezoelectric actuator. Although other materials, such as ZnO and PZT (Pb[Zr$_x$Ti$_{1-x}$]O$_3$), have stronger piezoelectric response, AlN has the key advantage of being compatible with the MOS fabrication flow. Other piezoelectrics contain fast-diffusing elements, which would contaminate the device and potentially the process tools.

Figure 2 shows the maps of dynamical strain $\delta\varepsilon_{ij}$ along a vertical cross section of the device, assuming that V_{RF} has the opposite phase
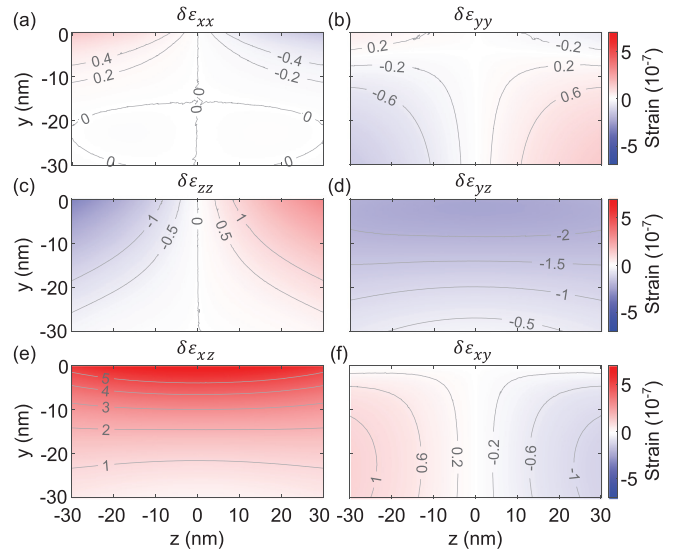
FIG. 2. Amplitudes of the periodic strain variation in the implantation window during the acoustic drive. The uniaxial strain components (a) $\delta\varepsilon_{xx}$, (b) $\delta\varepsilon_{yy}$, and (c) $\delta\varepsilon_{zz}$ and shear strain components (d) $\delta\varepsilon_{yz}$, (e) $\delta\varepsilon_{xz}$, and (f) $\delta\varepsilon_{xy}$ were calculated using the difference in strain between static gate voltages $V_{LD} = V_{LB} = V_{RD} = V_{RB} = 0$ V and peak driving amplitudes $V_{LD} = V_{LB} = 100$ mV and $V_{RD} = V_{RB} = -100$ mV. Shown are cross sections below the Si/SiO$_2$ interface in the center of the implantation window, located 30 nm from the SET top gate, as indicated in Fig. 1. Shear components $\delta\varepsilon_{yz}$ and $\delta\varepsilon_{xz}$ are the largest, indicating the strongest acoustic drive along $B_0 \parallel [100]$ axis.

on the left and right gates, and 100 mV peak amplitude. The model clearly shows that the shear strain $\delta\varepsilon_{yz}$ and $\delta\varepsilon_{xz}$ is the dominant component in the center of the device, as required for the fast acoustic drive as per Eq. (7).

To assess the strength of the electric contribution to the nuclear drive, we use COMSOL to model the amplitude of the electric field change δE_α produced by V_{RF}, plotted in Fig. 3. Our chosen device layout, having mirror symmetry around the $z = 0$ plane, and the applied V_{RF} having the opposite phase on the left and right gates, make δE_x and δE_y vanish in the center of the device.

The main result of our work is shown in Fig. 4. We calculate the nuclear Rabi frequencies predicted on the basis of both NAR [f^{NAR}, Eq. (7)] and NER [f^{NER}, Eq. (9)], using the parameters pertaining the $|5/2\rangle \leftrightarrow |7/2\rangle$ transition of a ^{123}Sb nucleus.[31] We find $f^{NAR} \approx 200$ Hz in a wide region of the device, at the shallow depths (≈ 5–10 nm) expected for donors implanted at ~ 10 keV energy.[41,42] For an ionized donor nuclear spin in isotopically enriched ^{28}Si, where the dephasing time is $T_{2n}^* \sim 0.1$ s, this value of f^{NAR} is sufficient to ensure high-quality coherent control.

Consistent with earlier experimental results,[31] we predict NER Rabi frequencies up to $f^{NER} \approx 1.5$ kHz. However, our design ensures that f^{NER} vanishes in the center of the device. This results in a ≈ 10 nm wide region, where $f^{NAR} \gg f^{NER}$ [Fig. 4(c)], i.e., wherein pure NAR can be observed. Capacitance triangulation methods[31,43] can locate individual donors within a ≈ 5 nm radius, allowing to identify which donors fall within the desired region.

A side effect of the application of strain is the local modulation of the host semiconductor's band structure, which can shift the electrochemical potential of the donor with respect to the SET. This must be minimized to ensure that the charge state of the donor does not change during the NAR drive. The effect of strain on the conduction band can be described via deformation potentials.[44] The dominant contribution is uniaxial strain that shifts the respective valleys by $\delta E_{\pm\alpha}^{CB} = \Xi_u \delta\varepsilon_{\alpha\alpha}$, where $\Xi_u = 10.5$ eV (Ref. 45) for silicon. We

(a) δE_x (b) δE_y (c) δE_z
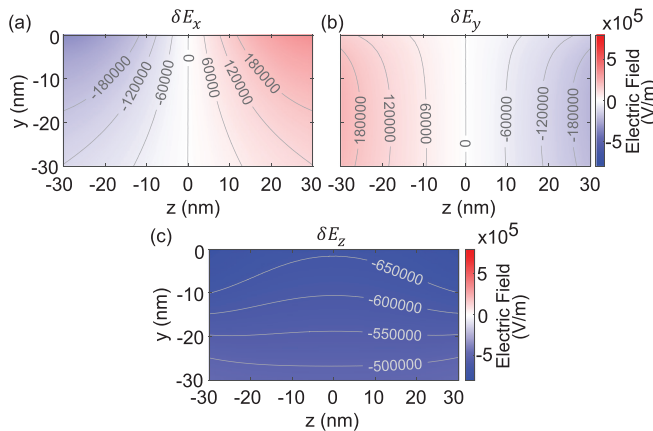
FIG. 3. Amplitudes of the electric field variation in the implantation window during the acoustic drive. The electric field components (a) δE_x, (b) δE_y, and (c) δE_z were calculated using the difference in electric fields between static gate voltages $V_{LD} = V_{LB} = V_{RD} = V_{RB} = 0$ V and peak driving amplitudes $V_{LD} = V_{LB} = 100$ mV and $V_{RD} = V_{RB} = -100$ mV. Shown is the same cross section as in Fig. 1. For the $B_0 \parallel$ [100] axis, the electric drive solely depends on δE_x and δE_y [see Eq. (9)], where both vanish at the center of the device.
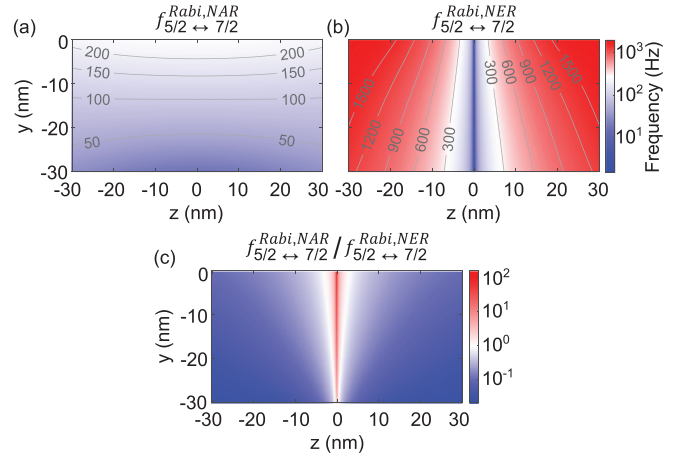
FIG. 4. The nuclear acoustic resonance (NAR) and nuclear electric resonance (NER) Rabi frequencies were calculated for the ^{123}Sb $|5/2\rangle \leftrightarrow |7/2\rangle$ transition with the B field oriented along the z-axis ([100] crystal axis) using Eqs. (7) and (9), respectively, with $R_{14} = 1.7 \times 10^{12}$ m^{-1} and $S_{44} = 5.9 \times 10^{22}$ V/m^2. (a) The NAR transition frequencies are uniformly distributed along the top region of the implantation window with a maximum of around 274 Hz. (b) The NER transition frequencies are minimal in the center of the implantation window (a minimum of around 1.5 Hz). (c) Their ratio $f_{5/2\leftrightarrow7/2}^{Rabi,NAR} / f_{5/2\leftrightarrow7/2}^{Rabi,NER}$ demonstrates the region, in which the NAR frequencies are greater than or comparable to the corresponding NER frequencies (a maximum ratio of around 160). A donor in the center of the implantation window ($z = 0$ nm) at a depth of $y = -5$ nm achieves $f_{5/2\leftrightarrow7/2}^{Rabi,NAR} = 190$ Hz while keeping $f_{5/2\leftrightarrow7/2}^{Rabi,NER} = 2.7$ Hz, corresponding to a ratio of $f_{5/2\leftrightarrow7/2}^{Rabi,NAR}/f_{5/2\leftrightarrow7/2}^{Rabi,NER} \approx 70$.

estimate a worst-case shift $\delta E_{SET}^{CB} = 0.525$ μeV at the SET, and $\delta E_{Donor} = 3.36$ μeV at the donor location. These values are orders of magnitude smaller than the electron confinement energies and the Zeeman splitting (the relevant scale for spin readout[36]) and small enough to be canceled by compensating voltages on the local gates, if required.

The calculations applied above to ^{123}Sb can be extended to any other $I > 1/2$ nucleus that can be individually addressed in silicon, by simply adapting the values of S_{11} and S_{44}. Table I presents values calculated using the projector-augmented wave formalism implemented in the Vienna Ab initio Simulation Package (VASP).[46–48] For each dopant species, the EFG at the relevant nucleus is calculated using a supercell of 512 atoms with one singly ionized dopant and a plane wave cutoff of 500 eV.[49] Having previously established a linear relationship between the EFG and strain up to 1% for ^{123}Sb,[31] we carry out all EFG calculations for 1% strain and determine the tensor components from Eq. (6). The numbers in Table I were computed using the SCAN exchange-correlation functional.[50] Using other exchange-correlation functionals, LDA[51] and PBE,[52] leads to a 2%–10% variation in S_{11} and S_{44} with no consistent trends among the species or functionals. As SCAN best reproduces the bulk elastic properties among the functionals considered, we consider those numbers to be the most reliable and have reported them.

In conclusion, our results show that a simple AlN piezoelectric actuator placed within a standard MOS-compatible donor qubit device is capable of driving coherent NAR transitions in a high-spin group-V donor in silicon. The choice of the device layout and magnetic field orientation with respect to the Si crystal axes allows us to suppress NER in the center of the device.

Our results indicate that, with the simple piezoelectric actuator modeled here, NAR is not expected to provide an advantage over NER for coherent nuclear drive. However, the experimental realization of this architecture will provide unique insights into the microscopic interplay between strain and spin qubits in silicon. The exceptional intrinsic spin coherence of nuclear spins in silicon, which results in resonance linewidths <10 Hz, translates into an equivalent spectroscopic resolution in the static (via f_Q) and dynamic (via $f^{\text{Rabi,NAR}}$) strain, detected by an atomic-scale probe. This information can be further correlated with other properties of the spin qubits hosted in the device such as spin relaxation times,[40] hyperfine,[11,13,14] and spin–orbit[54,55] couplings, valley effects,[56] or exchange interactions.[57–59] Such insights may even be used to validate a broad range of DFT models for semiconductor systems. Furthermore, the mechanical drive of a nuclear spin in an engineered silicon device will inform the prospect of coherently coupling nuclear spins to the quantized motion of high-quality mechanical resonators,[60,61] realizing a novel form of the hybrid quantum system.[15]

AUTHOR DECLARATIONS
Conflict of Interest

The authors have no conflicts to disclose.

DATA AVAILABILITY

The data that support the reported findings are available in FigShare at https://doi.org/10.6084/m9.figshare.16529208.v1, Ref. 62.

REFERENCES

[1]S. E. Thompson, G. Sun, Y. S. Choi, and T. Nishida, "Uniaxial-process-induced strained-Si: Extending the CMOS roadmap," IEEE Trans. Electron Devices **53**, 1010–1020 (2006).

[2]F. Schäffler, "High-mobility Si and Ge structures," Semicond. Sci. Technol. **12**, 1515 (1997).

[3]R. Hanson, L. P. Kouwenhoven, J. R. Petta, S. Tarucha, and L. M. Vandersypen, "Spins in few-electron quantum dots," Rev. Mod. Phys. **79**, 1217 (2007).

[4]F. A. Zwanenburg, A. S. Dzurak, A. Morello, M. Y. Simmons, L. C. Hollenberg, G. Klimeck, S. Rogge, S. N. Coppersmith, and M. A. Eriksson, "Silicon quantum electronics," Rev. Mod. Phys. **85**, 961 (2013).

[5]A. Chatterjee, P. Stevenson, S. De Franceschi, A. Morello, N. P. de Leon, and F. Kuemmeth, "Semiconductor qubits in practice," Nat. Rev. Phys. **3**, 157–177 (2021).

[6]F. Guinea, M. Katsnelson, and A. Geim, "Energy gaps and a zero-field quantum Hall effect in graphene by strain engineering," Nat. Phys. **6**, 30–33 (2010).

[7]C. Brüne, C. Liu, E. Novik, E. Hankiewicz, H. Buhmann, Y. Chen, X. Qi, Z. Shen, S. Zhang, and L. Molenkamp, "Quantum Hall effect from the topological surface states of strained bulk HgTe," Phys. Rev. Lett. **106**, 126803 (2011).

[8]T. Thorbeck and N. M. Zimmerman, "Formation of strain-induced quantum dots in gated semiconductor nanostructures," AIP Adv. **5**, 087107 (2015).

[9]J. Park, Y. Ahn, J. Tilka, K. Sampson, D. Savage, J. R. Prance, C. Simmons, M. Lagally, S. Coppersmith, M. Eriksson *et al.*, "Electrode-stress-induced nanoscale disorder in Si quantum electronic devices," APL Mater. **4**, 066102 (2016).

[10]P. C. Spruijtenburg, S. V. Amitonov, W. G. van der Wiel, and F. A. Zwanenburg, "A fabrication guide for planar silicon quantum dot heterostructures," Nanotechnology **29**, 143001 (2018).

[11]L. Dreher, T. A. Hilker, A. Brandlmaier, S. T. Goennenwein, H. Huebl, M. Stutzmann, and M. S. Brandt, "Electroelastic hyperfine tuning of phosphorus donors in silicon," Phys. Rev. Lett. **106**, 037601 (2011).

[12]D. P. Franke, F. M. Hrubesch, M. Künzl, H.-W. Becker, K. M. Itoh, M. Stutzmann, F. Hoehne, L. Dreher, and M. S. Brandt, "Interaction of strain and nuclear spins in silicon: Quadrupolar effects on ionized donors," Phys. Rev. Lett. **115**, 057601 (2015).

[13]J. Mansir, P. Conti, Z. Zeng, J. J. Pla, P. Bertet, M. W. Swift, C. G. Van de Walle, M. L. Thewalt, B. Sklenard, Y.-M. Niquet *et al.*, "Linear hyperfine tuning of donor spins in silicon using hydrostatic strain," Phys. Rev. Lett. **120**, 167701 (2018).

[14]J. Pla, A. Bienfait, G. Pica, J. Mansir, F. Mohiyaddin, Z. Zeng, Y.-M. Niquet, A. Morello, T. Schenkel, J. Morton *et al.*, "Strain-induced spin-resonance shifts in silicon devices," Phys. Rev. Appl. **9**, 044014 (2018).

[15]G. Kurizki, P. Bertet, Y. Kubo, K. Mølmer, D. Petrosyan, P. Rabl, and J. Schmiedmayer, "Quantum technologies with hybrid systems," Proc. Natl. Acad. Sci. **112**, 3866–3873 (2015).

[16]R. Manenti, A. F. Kockum, A. Patterson, T. Behrle, J. Rahamim, G. Tancredi, F. Nori, and P. J. Leek, "Circuit quantum acoustodynamics with surface acoustic waves," Nat. Commun. **8**, 975 (2017).

[17]A. D. O'Connell, M. Hofheinz, M. Ansmann, R. C. Bialczak, M. Lenander, E. Lucero, M. Neeley, D. Sank, H. Wang, M. Weides *et al.*, "Quantum ground state and single-phonon control of a mechanical resonator," Nature **464**, 697–703 (2010).

[18]M. V. Gustafsson, T. Aref, A. F. Kockum, M. K. Ekström, G. Johansson, and P. Delsing, "Propagating phonons coupled to an artificial atom," Science **346**, 207–211 (2014).

[19]Ö. Soykal, R. Ruskov, and C. Tahan, "Sound-based analogue of cavity quantum electrodynamics in silicon," Phys. Rev. Lett. **107**, 235502 (2011).

[20]A. Barfuss, J. Teissier, E. Neu, A. Nunnenkamp, and P. Maletinsky, "Strong mechanical driving of a single electron spin," Nat. Phys. **11**, 820–824 (2015).

[21]D. A. Golter, T. Oo, M. Amezcua, K. A. Stewart, and H. Wang, "Optomechanical quantum control of a nitrogen-vacancy center in diamond," Phys. Rev. Lett. **116**, 143602 (2016).

[22]D. Lee, K. W. Lee, J. V. Cady, P. Ovartchaiyapong, and A. C. B. Jayich, "Topical review: Spins and mechanics in diamond," J. Opt. **19**, 033001 (2017).

[23]S. Maity, L. Shao, S. Bogdanović, S. Meesala, Y.-I. Sohn, N. Sinclair, B. Pingault, M. Chalupnik, C. Chia, L. Zheng *et al.*, "Coherent acoustic control of a single silicon vacancy spin in diamond," Nat. Commun. **11**, 193 (2020).

[24]S. Maity, B. Pingault, G. Joe, M. Chalupnik, D. Assumpção, E. Cornell, L. Shao, and M. Lončar, "Coherent coupling of mechanics to a single nuclear spin," preprint arXiv:2107.10961 (2021).

[25]S. J. Whiteley, G. Wolfowicz, C. P. Anderson, A. Bourassa, H. Ma, M. Ye, G. Koolstra, K. J. Satzinger, M. V. Holt, F. J. Heremans *et al.*, "Spin–phonon interactions in silicon carbide addressed by Gaussian acoustics," Nat. Phys. **15**, 490–495 (2019).

[26]X. Zhang, C.-L. Zou, L. Jiang, and H. X. Tang, "Cavity magnomechanics," Sci. Adv. **2**, e1501286 (2016).

[27]S. Habraken, K. Stannigel, M. D. Lukin, P. Zoller, and P. Rabl, "Continuous mode cooling and phonon routers for phononic quantum networks," New J. Phys. **14**, 115004 (2012).

[28]R. Melcher, D. Bolef, and R. Stevenson, "Direct detection of F^{19} nuclear acoustic resonance in antiferromagnetic $RbMnF_3$," Phys. Rev. Lett. **20**, 453 (1968).

[29]R. Sundfors, "Experimental gradient-elastic tensors and chemical bonding in III-V semiconductors," Phys. Rev. B **10**, 4244 (1974).

[30]R. Sundfors, "Nuclear acoustic resonance of Ge^{73} in single-crystal germanium; interpretation of experimental gradient-elastic-tensor components in germanium and zinc-blende compounds," Phys. Rev. B **20**, 3562 (1979).

[31]S. Asaad, V. Mourik, B. Joecker, M. A. Johnson, A. D. Baczewski, H. R. Firgau, M. T. Mądzik, V. Schmitt, J. J. Pla, F. E. Hudson, *et al.*, "Coherent electrical control of a single high-spin nucleus in silicon," Nature **579**, 205–209 (2020).

[32]J. J. Pla, K. Y. Tan, J. P. Dehollain, W. H. Lim, J. J. Morton, F. A. Zwanenburg, D. N. Jamieson, A. S. Dzurak, and A. Morello, "High-fidelity readout and control of a nuclear spin qubit in silicon," Nature **496**, 334–338 (2013).

[33]K. Momma and F. Izumi, "Vesta 3 for three-dimensional visualization of crystal, volumetric and morphology data," J. Appl. Crystallogr. **44**, 1272–1276 (2011).

[34]A. Morello, C. Escott, H. Huebl, L. W. Van Beveren, L. Hollenberg, D. Jamieson, A. Dzurak, and R. Clark, "Architecture for high-sensitivity single-shot readout and control of the electron spin of individual donors in silicon," Phys. Rev. B **80**, 081307 (2009).

[35]A. Morello, J. J. Pla, P. Bertet, and D. N. Jamieson, "Donor spins in silicon for quantum technologies," Adv. Quantum Technol. **3**, 2000005 (2020).

[36]A. Morello, J. J. Pla, F. A. Zwanenburg, K. W. Chan, K. Y. Tan, H. Huebl, M. Möttönen, C. D. Nugroho, C. Yang, J. A. Van Donkelaar *et al.*, "Single-shot readout of an electron spin in silicon," Nature **467**, 687–691 (2010).

[37]J. Dehollain, J. Pla, E. Siew, K. Tan, A. Dzurak, and A. Morello, "Nanoscale broadband transmission lines for spin qubit control," Nanotechnology **24**, 015202 (2013).

[38]J. J. Pla, K. Y. Tan, J. P. Dehollain, W. H. Lim, J. J. Morton, D. N. Jamieson, A. S. Dzurak, and A. Morello, "A single-atom electron spin qubit in silicon," Nature **489**, 541–545 (2012).

[39]B. Hensen, W. W. Huang, C.-H. Yang, K. W. Chan, J. Yoneda, T. Tanttu, F. E. Hudson, A. Laucht, K. M. Itoh, T. D. Ladd *et al.*, "A silicon quantum-dot-coupled nuclear spin qubit," Nat. Nanotechnol. **15**, 13–17 (2020).

[40]S. B. Tenberg, S. Asaad, M. T. Mądzik, M. A. Johnson, B. Joecker, A. Laucht, F. E. Hudson, K. M. Itoh, A. M. Jakob, B. C. Johnson, *et al.*, "Electron spin relaxation of single phosphorus donors in metal-oxide-semiconductor nanoscale devices," Phys. Rev. B **99**, 205306 (2019).

[41]J. Van Donkelaar, C. Yang, A. Alves, J. McCallum, C. Hougaard, B. Johnson, F. Hudson, A. Dzurak, A. Morello, D. Spemann *et al.*, "Single atom devices by ion implantation," J. Phys.: Condens. Matter **27**, 154204 (2015).

[42]A. M. Jakob, S. G. Robson, V. Schmitt, V. Mourik, M. Posselt, D. Spemann, B. C. Johnson, H. R. Firgau, E. Mayes, J. C. McCallum *et al.*, "Deterministic single ion implantation with 99.87% confidence for scalable donor-qubit arrays in silicon," preprint arXiv:2009.02892 (2020).

[43]F. A. Mohiyaddin, R. Rahman, R. Kalra, G. Klimeck, L. C. Hollenberg, J. J. Pla, A. S. Dzurak, and A. Morello, "Noninvasive spatial metrology of single-atom devices," Nano Lett. **13**, 1903–1909 (2013).

[44]D. Wilson and G. Feher, "Electron spin resonance experiments on donors in silicon. III. Investigation of excited states by the application of uniaxial stress and their importance in relaxation processes," Phys. Rev. **124**, 1068 (1961).

[45]M. V. Fischetti and S. E. Laux, "Band structure, deformation potentials, and carrier mobility in strained Si, Ge, and SiGe alloys," J. Appl. Phys. **80**, 2234–2252 (1996).

[46]G. Kresse and J. Furthmüller, "Efficiency of *ab-initio* total energy calculations for metals and semiconductors using a plane-wave basis set," Comput. Mater. Sci. **6**, 15–50 (1996).

[47]G. Kresse and J. Furthmüller, "Efficient iterative schemes for *ab initio* total-energy calculations using a plane-wave basis set," Phys. Rev. B **54**, 11169 (1996).

[48]G. Kresse and D. Joubert, "From ultrasoft pseudopotentials to the projector augmented-wave method," Phys. Rev. B **59**, 1758 (1999).

[49]H. M. Petrilli, P. E. Blöchl, P. Blaha, and K. Schwarz, "Electric-field-gradient calculations using the projector augmented wave method," Phys. Rev. B **57**, 14690 (1998).

[50]J. Sun, A. Ruzsinszky, and J. P. Perdew, "Strongly constrained and appropriately normed semilocal density functional," Phys. Rev. Lett. **115**, 036402 (2015).

[51]D. M. Ceperley and B. J. Alder, "Ground state of the electron gas by a stochastic method," Phys. Rev. Lett. **45**, 566 (1980).

[52]J. P. Perdew, K. Burke, and M. Ernzerhof, "Generalized gradient approximation made simple," Phys. Rev. Lett. **77**, 3865 (1996).

[53]N. Stone, "Table of nuclear magnetic dipole and electric quadrupole moments," At. Data Nucl. Data Tables **90**, 75–176 (2005).

[54]J. Salfi, J. A. Mol, D. Culcer, and S. Rogge, "Charge-insensitive single-atom spin-orbit qubit in silicon," Phys. Rev. Lett. **116**, 246801 (2016).

[55]V. P. Michal, B. Venitucci, and Y.-M. Niquet, "Longitudinal and transverse electric field manipulation of hole spin-orbit qubits in one-dimensional channels," Phys. Rev. B **103**, 045305 (2021).

[56]B. Voisin, K. S. H. Ng, J. Salfi, M. Usman, J. C. Wong, A. Tankasala, B. C. Johnson, J. C. McCallum, L. Hutin, B. Bertrand, M. Vinet, N. Valanoor, M. Y. Simmons, R. Rahman, L. C. L. Hollenberg, and S. Rogge, "Valley population of donor states in highly strained silicon," arXiv:2109.08540 [cond-mat.mes-hall] (2021).

[57]B. Voisin, J. Bocquel, A. Tankasala, M. Usman, J. Salfi, R. Rahman, M. Simmons, L. Hollenberg, and S. Rogge, "Valley interference and spin exchange at the atomic scale in silicon," Nat. Commun. **11**, 6124 (2020).

[58]K. W. Chan, H. Sahasrabudhe, W. Huang, Y. Wang, H. C. Yang, M. Veldhorst, J. C. Hwang, F. A. Mohiyaddin, F. E. Hudson, K. M. Itoh *et al.*, "Exchange coupling in a linear chain of three quantum-dot spin qubits in silicon," Nano Lett. **21**, 1517–1522 (2021).

[59]M. T. Mądzik, A. Laucht, F. E. Hudson, A. M. Jakob, B. C. Johnson, D. N. Jamieson, K. M. Itoh, A. S. Dzurak, and A. Morello, "Conditional quantum operation of two exchange-coupled single-donor spin qubits in a mos-compatible silicon device," Nat. Commun. **12**, 181 (2021).

[60]S. Ghaffari, S. A. Chandorkar, S. Wang, E. J. Ng, C. H. Ahn, V. Hong, Y. Yang, and T. W. Kenny, "Quantum limit of quality factor in silicon micro and nano mechanical resonators," Sci. Rep. **3**, 3244 (2013).

[61]A. H. Safavi-Naeini, D. Van Thourhout, R. Baets, and R. Van Laer, "Controlling phonons and photons at the wavelength scale: Integrated photonics meets integrated phononics," Optica **6**, 213–232 (2019).

[62]L. O'Neill, B. Joecker, A. Baczewski, and A. Morello, "Engineering local strain for single-atom nuclear acoustic resonance in silicon–Datasets," FigShare (2021). https://doi.org/10.6084/m9.figshare.16529208.v1